MAGNETISM

Skyrmion lattice with a giant topological Hall effect in a frustrated triangular-lattice magnet

Takashi Kurumaji[1]*, Taro Nakajima[1], Max Hirschberger[1], Akiko Kikkawa[1], Yuichi Yamasaki[1,2,3], Hajime Sagayama[4], Hironori Nakao[4], Yasujiro Taguchi[1], Taka-hisa Arima[1,5], Yoshinori Tokura[1,6]

Geometrically frustrated magnets can host complex spin textures, leading to unconventional electromagnetic responses. Magnetic frustration may also promote topologically nontrivial spin states such as magnetic skyrmions. Experimentally, however, skyrmions have largely been observed in noncentrosymmetric lattice structures or interfacial symmetry-breaking heterostructures. Here, we report the emergence of a Bloch-type skyrmion state in the frustrated centrosymmetric triangular-lattice magnet Gd_2PdSi_3. We observed a giant topological Hall response, indicating a field-induced skyrmion phase, which is further corroborated by the observation of in-plane spin modulation probed by resonant x-ray scattering. Our results may lead to further discoveries of emergent electrodynamics in magnetically frustrated centrosymmetric materials.

In geometrically frustrated magnets, where competing interactions among localized spins cannot be simultaneously satisfied, conventional magnetic orders are suppressed. Consequently, spins strongly fluctuate and can form a disordered state known as a spin-liquid state (*1*) or occasionally find a route to various spin textures, including spin-spiral orders or more-complex noncoplanar orders (*2*, *3*). These spin states are mutually competing in energy, resulting in a complex magnetic phase diagram with respect to temperature, magnetic field, and pressure. An emerging spin state can be characterized from the perspective of geometrical correlation of spin vectors ($\mathbf{S}_i$) on neighboring sites (i, j, k) in a lattice. For example, the vector spin chirality $\mathbf{S}_i \times \mathbf{S}_j$ describes the handedness of a spin spiral (*4*), and the scalar spin chirality $\mathbf{S}_i \cdot (\mathbf{S}_j \times \mathbf{S}_k)$ is connected to time-reversal symmetry breaking (*5*, *6*). These composite spin parameters couple with charge degrees of freedom in a correlated electron system, causing unconventional electromagnetic responses (*7*–*10*). Exploration of previously unknown spin textures via magnetic frustration has been one of the recent central directions in condensed matter physics.

Spin configurations are characterized by topological numbers, which remain intact under local deformation or weak fluctuations (*11*). Since the discovery of magnetic skyrmion states in chiral magnets (*12*, *13*), this concept has attracted growing interest. The magnetic skyrmion is a vortex-like nanometric spin structure that carries an integer topological number describing how many times magnetic moments within a skyrmion wrap a sphere (*14*). This quantization defines the particle nature of this spin texture with sensitivity to the electronic current and external electric and magnetic fields, highlighting the potential of magnetic skyrmions as information carriers (*15*). Extensive studies have successfully identified skyrmion-hosting materials in the form of both bulk compounds (*16*) and multilayer thin-film structures (*17*). From those, one can establish an empirical design principle for skyrmions (*18*, *19*): They appear in crystallographic lattice structures that lack inversion symmetry in or at the interfaces. These asymmetries cause the relativistic Dzyaloshinskii-Moriya (DM) interaction (*20*, *21*), which inherently prefers twisted spin configurations. More recently, this dogma has been challenged in theories (*22*–*24*) that propose spontaneous symmetry breaking by stabilizing the skyrmion state in centrosymmetric lattices via magnetic frustration. However, experimental realization and observation of unconventional electronic responses have remained elusive.

Here, we demonstrate that the metallic magnet Gd_2PdSi_3, composed of a triangular-lattice network of Gd atoms (Fig. 1A) in the centrosymmetric hexagonal structure, hosts a skyrmion-lattice (SkL) state upon the application of a magnetic field (H) perpendicular to the triangular-lattice plane, which is robust down to the lowest measured temperature. The transition into the topological spin state is characterized by a prominent topological Hall response (*25*, *26*), in sharp contrast to the adjacent magnetic phases. Using resonant x-ray scattering (RXS), we identify the long-range order of Gd spins modulated in the triangular lattice plane. The spin texture of the field-induced SkL phase is consistent with a triangular-lattice of Bloch-type skyrmions (Fig. 1B).

Gd_2PdSi_3 belongs to a family of rare-earth intermetallics of the form R_2PdSi_3 (R, rare-earth element) (*27*). Its crystal structure is derived from the simple AlB_2-type structure, with a triangular-lattice of R atoms sandwiching a nonmagnetic honeycomb-lattice layer composed of Pd and Si atoms (Fig. 1A). Owing to the difference in atomic size, Si and Pd atoms order into a superstructure along both in- and out-of-plane directions (*28*), whereas the overall structure retains centrosymmetry (fig. S1A). This excludes the DM interaction as a source of the skyrmion state. Instead, the Ruderman-Kittel-Kasuya-Yosida (RKKY)–type interaction among the local 4f moments dominates (*29*–*31*); RKKY interactions on the triangular network of 4f moments in R_2PdSi_3 are moderately frustrated (*32*) and show rich magnetic phases, including modulated structures (*33*). Specifically, in Gd_2PdSi_3, metamagnetic transitions have been observed under a magnetic field applied perpendicular to the triangular lattice, accompanied by nonmonotonic variations of longitudinal and transverse transport properties (*34*). These features suggest strong coupling between conduction electrons and Gd spins and indicate that unconventional spin structures may emerge in the triangular-lattice network of Gd 4f moments.

We first compare the magnetic phase diagram determined by the ac susceptibility (χ') for $H \| c$ in Gd_2PdSi_3 (Fig. 1C) with the contour mapping of the topological response of each phase probed by the topological Hall resistivity ρ_{yx}^{T} (Fig. 1D). Owing to the topological nature of skyrmions, they show characteristic emergent electrodynamic responses (*14*). In metallic materials, in particular, the scalar spin chirality of skyrmions acts like a fictitious magnetic field, which generates a transverse motion of electrons; this is known as the topological Hall effect (THE) (*25*, *26*, *35*). The transverse resistivity ρ_{yx} is generally made up of three components

$$\rho_{yx} = R_0 B + R_S M + \rho_{yx}^{T} \quad (1)$$

where the first and second terms are the normal and anomalous Hall resistivities proportional to the magnetic induction field B and the magnetization M, respectively, and the third term represents the topological component. Because the first two terms can be determined from magnetization measurements, ρ_{yx}^{T} can be extracted reliably and is considered a good probe for the existence of skyrmions or related topological spin states in various materials (*36*). As shown in Fig. 1C, peaks in χ' with respect to H (fig. S2) define the phase boundaries for the three magnetic phases (IC-1, A, and IC-2) in addition to the

[1]RIKEN Center for Emergent Matter Science (CEMS), Wako 351-0198, Japan. [2]Research and Services Division of Materials Data and Integrated System (MaDIS), National Institute for Materials Science (NIMS), Tsukuba 305-0047, Japan. [3]PRESTO, Japan Science and Technology Agency (JST), Kawaguchi 332-0012, Japan. [4]Institute of Materials Structure Science, High Energy Accelerator Research Organization, Tsukuba, Ibaraki 305-0801, Japan. [5]Department of Advanced Materials Science, University of Tokyo, Kashiwa 277-8561, Japan. [6]Department of Applied Physics, University of Tokyo, Tokyo 113-8656, Japan.
*Corresponding author. Email: takashi.kurumaji@riken.jp

paramagnetic (PM) state (*34*). In the *H*-*T* phase diagram, we overlay the contour plot of ρ_{yx}^{T} (Fig. 1D), which is deduced from the Hall resistivity measurements. The enhanced topological Hall signal appearing exclusively in the *A*-phase region suggests that in Gd_2PdSi_3 the application of *H* induces topological phase transitions in the context of spin textures. The magnitude of the THE at the lowest temperature is as large as 2.6 microhm·cm, which is one or two orders of magnitude larger than that in other skyrmion-hosting materials such as MnSi (40 nanohm·cm under high pressure) (*25*, *26*, *35*, *37*) and FeGe (0.16 microhm·cm in a thin film) (*38*). This must be partly caused by a shorter wavelength of the spin modulation (~2.5 nm) (fig. S5), which squeezes the emergent magnetic flux of a skyrmion, in contrast to the relatively large size of skyrmions (10 to 100 nm) in typical noncentrosymmetric (chiral or polar) magnets (*36*).

To corroborate the observation of the THE in the *A* phase, we show a typical ρ_{yx}–*H* curve together with the *M* for $H \| c$ at 2 K (Fig. 2A). A sharp positive enhancement of ρ_{yx} is apparent in the region between two stepwise changes of *M*, defining the first-order–like transitions to and from the *A* phase. On the contrary, in the IC-2 phase and higher-field region, ρ_{yx} stays negative with nearly field-linear behavior, at least up to 140 kOe (fig. S3A), where *M* is 13.7 μ_B/f.u. (where μ_B is the Bohr magneton and f.u. is formula unit), approaching the saturation value expected for the value of local Gd moment. In principle, this nearly saturated phase hosts a topologically trivial spin arrangement, allowing us to describe the Hall response with the first two terms in Eq. 1. The black solid line in Fig. 2A shows the fit to the high-field data of ρ_{yx}. The fitting quality is excellent for all measured temperatures (fig. S3A), which allows us to unambiguously extract ρ_{yx}^{T} from ρ_{yx} (Figs. 2B and 1C). The quality of the fit is not substantially affected by using a different formula—e.g., assuming skew scattering type anomalous Hall effect (fig. S4). Figure 2C shows the evolution of the peak in ρ_{yx}^{T} with temperature. Continuous decrease of ρ_{yx}^{T} toward zero around 20 K suggests that this response is affected by the magnitude of the molecular field from 4f moment on the conduction electron through an f-d coupling, consistent with the scalar spin chirality model for the THE (*35*). The effective magnetic field (B_{eff}) for the maximum ρ_{yx}^{T} is around −39 T (*39*), which is a factor of 0.07(≡*P*) smaller than the bare emergent magnetic field (B_{em} ~ −570 T) estimated from the skyrmion density. The polarization factor *P* is one order of magnitude smaller than those in MnSi under pressure (*P* ~ 0.25 to 0.38) and slightly-doped $Mn_{1-x}Fe_xSi$ (*P* ~ 0.3 to 0.45) (*37*). This may be caused by the moderate f-d coupling in the present rare-earth system as compared with the strong d-d coupling in transition metal compounds.

To further examine the nature of the SkL state in the *A* phase, we present the Hall resistivity as a function of the angle between *H* and the *c* axis in the experimental configuration illustrated in the inset of Fig. 2D. At $\phi = 0°(H \| c)$ with *H* = 9.9 kOe in the *A* phase, ρ_{yx} starts from a large positive value. As *H* rotates clockwise away from the *c* axis, the value of ρ_{yx} remains flat until it experiences an abrupt drop to near zero at around $\phi = 45°$. A hysteresis with a width of ~15° is observed between clockwise and counterclockwise rotation scans of *H*, pointing to the first-order nature of this *H*-direction–sensitive phase transition. This should be compared to thin-film systems (*40*, *41*), in which the SkL is confined in a two-dimensional space and survives only when *H* is oriented nearly perpendicular to the lattice plane. Similar behavior may be expected for the present system composed of stacked triangular-lattice layers. The above observation provides a measure of the topological number for the spin texture where the topological Hall signal sharply transitions from finite to zero upon the destabilization of the SkL state. In contrast, at *H* = 40 kOe, far above the upper critical field of the *A* phase, a smooth evolution of ρ_{yx} is observed with negligible hysteresis. This high-field ρ_{yx}, the absolute magnitude of which is much smaller than the SkL signal, follows cosϕ (black solid line in Fig. 2D), indicating that *M* closely follows the

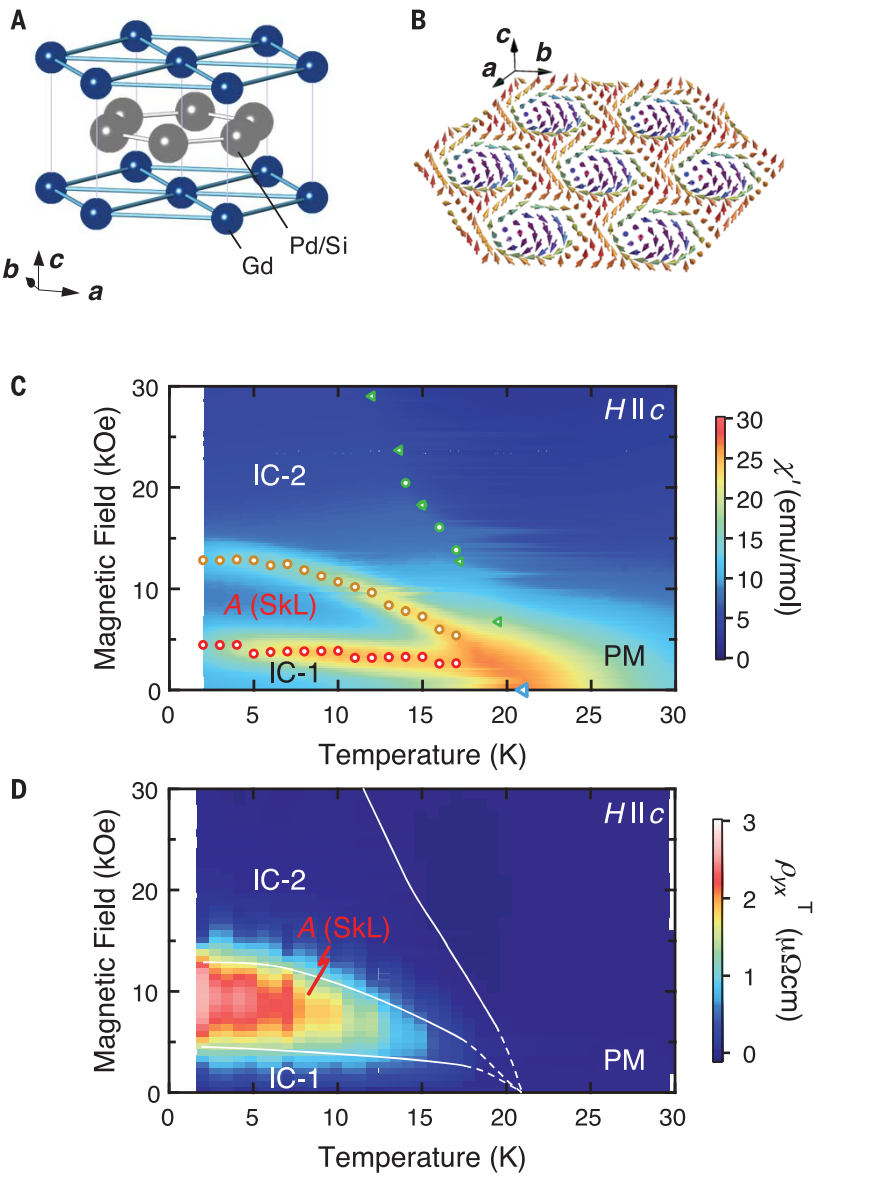

Fig. 1. Phase diagram and THE in Gd_2PdSi_3. (**A**) Basic AlB_2-type crystal structure for Gd_2PdSi_3. (**B**) Illustration of the spin texture in the SkL state. Each arrow indicates a magnetic moment at each Gd site. (**C** and **D**) Contour plot of (C) χ′ and (D) ρ_{yx}^{T} for $H \| c$ (see text for definition). *A* represents the SkL phase and PM the paramagnetic phase. IC-1 and IC-2 denote incommensurate spin-state phases in near-zero and high-field regions, respectively. Circular (triangular) symbols were determined by a peak or a kink in the χ′-*H* (χ′-*T*) scan (fig. S2). emu, electromagnetic units; mol, molar.

rotating H and that the projections of M and B to the c axis produce the first two terms in Eq. 1 as dominant contributions to ρ_{yx} outside the A-phase region.

Having identified the emergence of a topological electromagnetic response in the A phase, we examined the Gd spin structure under H along the c axis by means of the magnetic RXS in resonance with the Gd L_2 edge. We observed the magnetic modulation along in-plane directions represented by the reciprocal-space vector $\mathbf{Q}_1 = (q, 0, 0)$ [and equivalent $\mathbf{Q}_2 = (0, -q, 0)$ and $\mathbf{Q}_3 = (q, -q, 0)$] in the magnetically ordered phase (*39*). Here, q (~ 0.14 reciprocal lattice unit) is the magnetic modulation wave number. In Fig. 3, A and B, we show M and q, respectively, as a function of H, which is applied along the c axis; the data were taken at 5 K. To define the phase boundary for each phase, we show the difference ΔM between the measurements of M for the H-increasing and H-decreasing scans (Fig. 3A). In the IC-1 phase, q is almost independent of H and starts to gradually increase on entering the A phase and, furthermore, the IC-2 state. Despite the clear first-order nature for each transition (vertical gray lines), q shows merely a weak kink at each phase boundary and changes only 4% in total between 0 Oe in the IC-1 phase and 20 kOe in the IC-2 phase. The orientation of the Q vectors with respect to the triangular lattice does not change across these metamagnetic transitions. This restricts the candidate spin textures for each phase to the spin modulations with one or several equivalent Q vectors plus a component of homogeneous magnetization ($q = 0$) along the c axis. This is consistent with the intermediate-field SkL state, which can be seen as a superposition of three spiral spin modulations with their magnetic modulation vectors lying in the triangular-lattice plane and pointing 120° away from each other.

Figure 3C shows the H dependence of the scattering intensities for respective satellite peaks for the three Q vectors measured around a Bragg spot (2, 2, 0) in the H-decreasing scan. Starting from the high-field IC-2 phase region (10 kOe < H < 20 kOe), we observed that the intensity for one of the Q vectors (I_{Q_2}) is markedly weak compared with I_{Q_1} and I_{Q_3}. A fanlike structure (fig. S7A) provides a good explanation for this feature as follows. Polarization analysis of the scattered x-ray, which enables decomposition of the in-plane ($\mathbf{m}_\perp$) and out-of-plane (m_z) components of the modulated magnetic moment (*39*), reveals the negligibly weak modulating m_z component (fig. S6B) for the magnetic structure of the IC-2 state. We thus propose that a possible magnetic structure for the IC-2 state is a fanlike or a transverse conical structure (fig. S7, A and B), both of which lack global scalar spin chirality in accord with the absence of a topological contribution in ρ_{yx}. Of the two proposed magnetic structures, the fan model gives a better fit to the observed intensity, although both fits deviate from experimental observations. The observed imbalance of the scattering intensity among the three Q domains is suggestive of the single-Q nature of this phase and stems perhaps from residual strains on the sample induced by shaping and attaching it on the sample holder (*42*).

With decreasing H (Fig. 3C), the intensities for all the three Q vectors show a stepwise increase upon entering the A phase. Such a simultaneous increase of intensity for every Q is associated with the developing m_z (modulation component), as shown in Fig. 3D, which is absent in the IC-2 phase. This fact points to a noncoplanar spin texture in the topological A phase. When H decreases further (Fig. 3C), the intensity for each Q vector is almost unchanged, whereas a prominent peak in ΔM (Fig. 3A) suggests a first-order phase transition from the A phase to the IC-1 phase. The polarization analysis reveals the presence of an m_z component (fig. S6A) comparable with that of the A phase, suggesting a similarity of the spin configurations for both phases.

Looking back to the polarization analysis for the A phase (Fig. 3D), the intensity $I_{\pi-\pi'}$ for the π-π' channel ($\propto m_z^2$) is of nearly the same magnitude for all $\mathbf{Q}_i$, consistent with the triple-Q nature of the skyrmion state. $I_{\pi-\sigma'}$ ($\propto (\mathbf{m}_\perp \cdot \mathbf{k}_i)^2$) is, on the other hand, correlated with $\mathbf{m}_\perp$ to show clear $\mathbf{Q}_i$ dependence. For the Bloch-type SkL state, the spin texture is composed of a superposition of the three proper-screw spin modulations (Fig. 3E), where $\mathbf{m}_\perp$ is perpendicular to each $\mathbf{Q}_i$ vector (Fig. 3E, inset). As shown in Fig. 3F and the corresponding inset, the direction of $\mathbf{Q}_2$ is particularly closer to $\mathbf{k}_i$ than are the directions of $\mathbf{Q}_1$ and $\mathbf{Q}_3$—i.e., the direction of $\mathbf{m}_\perp$ for $\mathbf{Q}_2$ is closer to the direction normal to $\mathbf{k}_i$ than those for $\mathbf{Q}_1$ and $\mathbf{Q}_3$. This feature is consistent with the $\mathbf{Q}_i$ dependence of $I_{\pi-\sigma'}$. Furthermore, a quantitative comparison between the calculated and observed intensities reveals that the magnetic structures in the A phase can be reproduced by hybridization of the three proper screws with equivalent amplitude plus the uniform moment along z (fig. S6C), consistent with the picture of the Bloch-type SkL state. This spin texture spontaneously breaks the inversion symmetry and potentially hosts domains for handedness of skyrmions. Preference for the Bloch-type spin configuration over the Néel or the antiskyrmion type is consistent with the effect of the dipole-dipole interaction (*14*, *43*), which is generally substantial in Gd compounds.

The scattering intensities in the IC-1 state (fig. S6, A and C) suggest that the IC-1 state may also be of triple-Q nature but forms a spin texture topologically distinct from that of the A phase. A degree of freedom for the phase (φ_i) remains among the three helical modulations

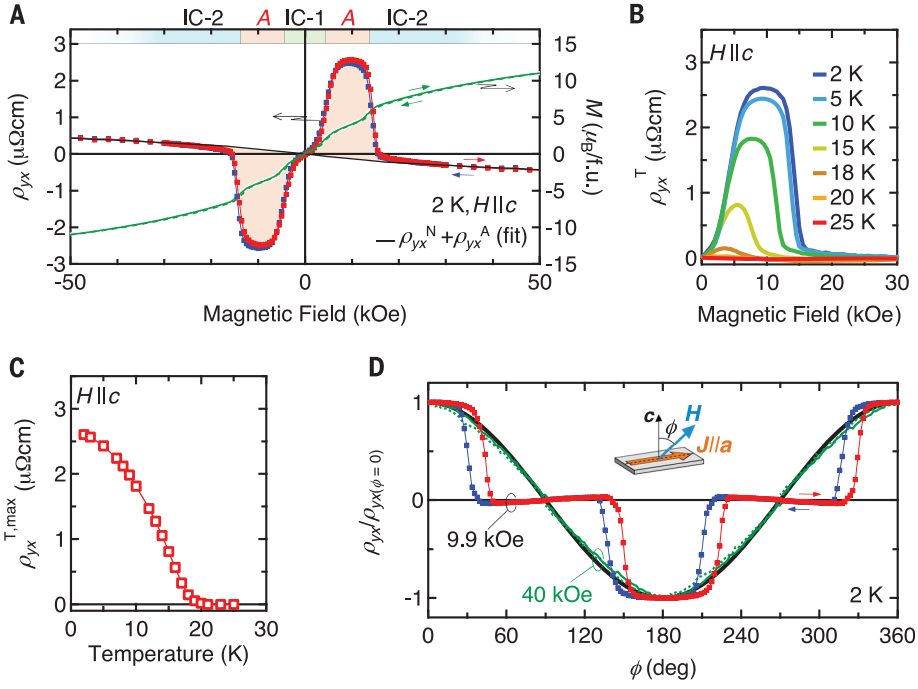

Fig. 2. Temperature and angular dependence of the THE in Gd_2PdSi_3. (**A**) H dependence of ρ_{yx} (left y axis) and M (right y axis) for $H \| c$ at 2 K. The red (blue) curve represents the H-increasing (H-decreasing) scan. The black curve indicates the sum of the normal (ρ_{yx}^N) and anomalous (ρ_{yx}^A) components of Hall resistivity. μ_B, Bohr magneton; f.u., formula unit. (**B**) H dependence of topological Hall component ρ_{yx}^T at various temperatures. (**C**) Temperature dependence of the maximum values of ρ_{yx}^T ($\rho_{yx}^{T,max}$). (**D**) Normalized transverse resistivity at 2 K with H rotating in the ac plane. Red (blue) symbols and green solid (dashed) line are in a (counter)clockwise rotation. The inset defines the rotation angle ϕ. The reference line cosϕ is shown by the black solid line.

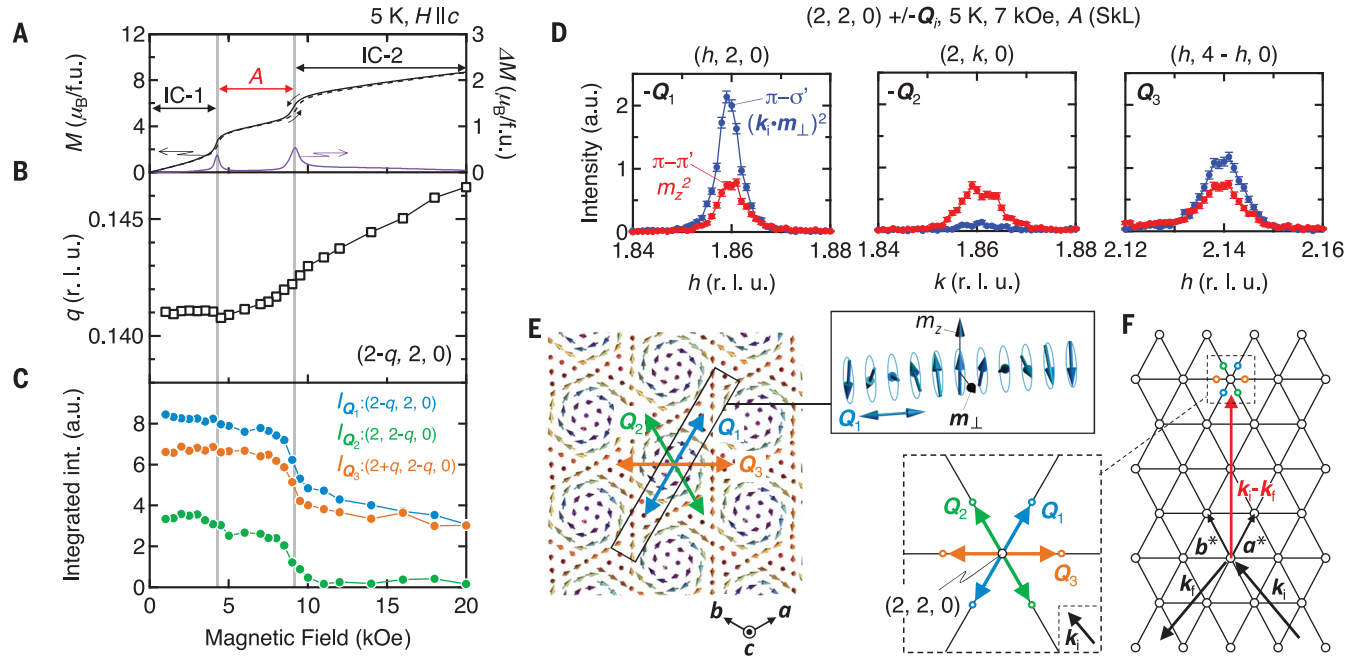

Fig. 3. Analysis of spin textures by RXS. (**A**) *H* dependence of *M* in *H*-increasing (black dashed line) and *H*-decreasing (black solid line) sweeps and the difference between them (Δ*M*, purple solid line). (**B** and **C**) Plots of (B) *q* and (C) integrated intensity for each magnetic satellite peak at $\mathbf{Q}_i$ (*i* = 1, 2, 3) around the Bragg peak (2, 2, 0), measured at 5 K and in an *H*-decreasing sweep. r.l.u., reciprocal lattice units; a.u., arbitrary units. (**D**) Intensity profile of magnetic reflection of each polarization channel for each (−)$\mathbf{Q}_i$ at 5 K with *H*||*c* of 7 kOe in the *A* (SkL)–phase region. Red [blue] circles denote the π-π′ [π-σ′] channel, which is approximately proportional to the m_z^2 [$(\mathbf{k}_i \cdot \mathbf{m}_\perp)^2$] (*39*). π (σ) corresponds to the x-ray polarization parallel (perpendicular) to the (0, 0, *L*) plane. Error bars indicate 1 SD. (**E**) Schematic real-space texture for the Bloch-type SkL state with the definition of $\mathbf{Q}_i$ (*i* = 1, 2, 3). (Inset) Proper-screw–type modulation component propagating along $\mathbf{Q}_1$. m_z and $\mathbf{m}_\perp$ represent the respective *c*-axis and *ab*-plane components of the magnetic moments. (**F**) Illustration of x-ray scattering condition in the reciprocal space. The inset shows a magnified view around (2, 2, 0), indicating the relationship between $\mathbf{Q}_i$ and $\mathbf{k}_i$.

(*39*). When the φ_i for each $\mathbf{Q}_i$ vector is 0 (mod 2π), the triple-*Q* state is equivalent to the Bloch-type SkL state, as exemplified by the *A* phase. For $\varphi_i = \pi/6$, the triple-*Q* state is composed of a triangular-lattice of merons and antimerons (fig. S7C) with no net scalar spin chirality at zero field; this is compatible with the observed features for the IC-1 state (*39*). The possible emergence of a triple-*Q* zero-field ground state (IC-1) may be a notable difference from the conventional noncentrosymmetric skyrmion-hosting systems, which typically show a single-*Q* helical state as the zero-field state (*36*). We also note unconventional features beyond the conventional helical or conical state in the IC-1 phase. As shown in Fig. 2B, ρ_{yx}^{T} starts to gradually increase from zero field before a steep increase characterizing the transition to the skyrmion state, which can be explained by the proposed noncoplanar nature in the IC-1 state: The meron-antimeron lattice can show an *H*-induced scalar spin chirality (*39*).

According to existing theories, skyrmion phase down to the lowest temperature is enabled by the magnetic frustration with support from additional effects, such as magnetic anisotropy owing to the spin-orbit coupling (*23*, *44*) and higher-order RKKY-like interaction (*24*). Notably, it is predicted that the latter mechanism can stabilize a zero-field multiple-*Q* state (albeit not identical with the present IC-1 state) (*45*), suggesting that nearly degenerate multiple-*Q* orders may exist in the ground state of the RKKY-based intermetallics. We observe that the magnetic structure for the IC-1 phase shows a certain ellipticity of the spin-spiral form (fig. S9), which suggests that weak easy-plane anisotropy may play a role in stabilizing the IC-1 state.

In addition to the enhanced THE, it has been theoretically predicted that the skyrmion in a centrosymmetric lattice shows distinctive properties, such as the compatible formation of antiskyrmion with skyrmion (*22*, *23*) and the helicity-dependent current responses (*43*, *44*). These properties provide the skyrmions as individual particles with internal degrees of freedom, which are absent in noncentrosymmetric systems with innate chirality or polarity. The conduction-electron–mediated competing magnetic interactions on a geometrically frustrated lattice will provide a platform for emergent electrodynamics owing to topological spin textures and will provide a link between the concepts of spin topology and magnetic frustration.

REFERENCES AND NOTES

1. L. Balents, *Nature* **464**, 199–208 (2010).
2. H. T. Diep, *Frustrated Spin Systems* (World Scientific, 2004).
3. C. Lacroix, P. Mendels, F. Mila, Eds., *Introduction to Frustrated Magnetism* (Springer Series in Solid State Sciences, vol. 164, Springer, 2011).
4. V. Simonet, M. Loire, R. Ballou, *Eur. Phys. J. Spec. Top.* **213**, 5–36 (2012).
5. V. Kalmeyer, R. B. Laughlin, *Phys. Rev. Lett.* **59**, 2095–2098 (1987).
6. X. G. Wen, F. Wilczek, A. Zee, *Phys. Rev. B* **39**, 11413–11423 (1989).
7. S.-W. Cheong, M. Mostovoy, *Nat. Mater.* **6**, 13–20 (2007).
8. Y. Taguchi, Y. Oohara, H. Yoshizawa, N. Nagaosa, Y. Tokura, *Science* **291**, 2573–2576 (2001).
9. Y. Machida, S. Nakatsuji, S. Onoda, T. Tayama, T. Sakakibara, *Nature* **463**, 210–213 (2010).
10. C. D. Batista, S.-Z. Lin, S. Hayami, Y. Kamiya, *Rep. Prog. Phys.* **79**, 084504 (2016).
11. H. B. Braun, *Adv. Phys.* **61**, 1–116 (2012).
12. S. Mühlbauer *et al.*, *Science* **323**, 915–919 (2009).
13. X. Z. Yu *et al.*, *Nature* **465**, 901–904 (2010).
14. N. Nagaosa, Y. Tokura, *Nat. Nanotechnol.* **8**, 899–911 (2013).
15. A. Fert, V. Cros, J. Sampaio, *Nat. Nanotechnol.* **8**, 152–156 (2013).
16. A. Bauer, C. Pfleiderer, *Generic Aspects of Skyrmion Lattices in Chiral Magnets* (Springer Series in Materials Science, vol. 228, Springer, 2016).
17. W. Jiang *et al.*, *Phys. Rep.* **704**, 1–49 (2017).
18. A. N. Bogdanov, D. A. Yablonskii, *Sov. Phys. JETP* **68**, 101–103 (1989).
19. A. Bogdanov, A. Hubert, *J. Magn. Magn. Mater.* **138**, 255–269 (1994).
20. I. Dzyaloshinskii, *J. Phys. Chem. Solids* **4**, 241–255 (1958).
21. T. Moriya, *Phys. Rev.* **120**, 91–98 (1960).
22. T. Okubo, S. Chung, H. Kawamura, *Phys. Rev. Lett.* **108**, 017206 (2012).
23. A. O. Leonov, M. Mostovoy, *Nat. Commun.* **6**, 8275 (2015).
24. S. Hayami, R. Ozawa, Y. Motome, *Phys. Rev. B* **95**, 224424 (2017).

25. M. Lee, W. Kang, Y. Onose, Y. Tokura, N. P. Ong, *Phys. Rev. Lett.* **102**, 186601 (2009).
26. A. Neubauer *et al*., *Phys. Rev. Lett.* **102**, 186602 (2009).
27. P. A. Kotsanidis, J. K. Yakinthos, E. Gamari-Seale, *J. Magn. Magn. Mater.* **87**, 199–204 (1990).
28. F. Tang *et al*., *Phys. Rev. B* **84**, 104105 (2011).
29. M. A. Ruderman, C. Kittel, *Phys. Rev.* **96**, 99–102 (1954).
30. T. Kasuya, *Prog. Theor. Phys.* **16**, 45–57 (1956).
31. K. Yosida, *Phys. Rev.* **106**, 893–898 (1957).
32. D. S. Inosov *et al*., *Phys. Rev. Lett.* **102**, 046401 (2009).
33. A. Szytuła *et al*., *J. Magn. Magn. Mater.* **202**, 365–375 (1999).
34. S. R. Saha *et al*., *Phys. Rev. B* **60**, 12162–12165 (1999).
35. R. Ritz *et al*., *Phys. Rev. B* **87**, 134424 (2013).
36. N. Kanazawa, S. Seki, Y. Tokura, *Adv. Mater.* **29**, 1603227 (2017).
37. B. J. Chapman, M. G. Grossnickle, T. Wolf, M. Lee, *Phys. Rev. B* **88**, 214406 (2013).
38. S. X. Huang, C. L. Chien, *Phys. Rev. Lett.* **108**, 267201 (2012).
39. See materials and methods and supplementary text.
40. T. Yokouchi *et al*., *Phys. Rev. B* **89**, 064416 (2014).
41. Y. Ohuchi *et al*., *Phys. Rev. B* **91**, 245115 (2015).
42. T. Inami, N. Terada, H. Kitazawa, O. Sakai, *J. Phys. Soc. Jpn.* **78**, 084713 (2009).
43. X. Zhang *et al*., *Nat. Commun.* **8**, 1717 (2017).
44. S.-Z. Lin, S. Hayami, *Phys. Rev. B* **93**, 064430 (2016).
45. R. Ozawa, S. Hayami, Y. Motome, *Phys. Rev. Lett.* **118**, 147205 (2017).
46. T. Kurumaji *et al*., Skyrmion in frustrated triangular-lattice, Version 1.0, Zenodo, (2019); http://doi.org/10.5281/zenodo.3240669.

ACKNOWLEDGMENTS

We thank X. Z. Yu for efforts on Lorentz transmission electron microscopy experiments and L. Ye, K. S. Okada, S. Hayami, H. Ishizuka, Y. Motome, and N. Nagaosa for helpful discussions. **Funding:** X-ray scattering measurements were performed under the approval of the Photon Factory Program Advisory Committee (proposal no. 2015S2-007) at the Institute of Material Structure Science, High Energy Accelerator Research Organization (KEK). This research was supported in part by Grant-in-Aid for Scientific Research (S) no. 24224009, Grant-In-Aid for Young Scientists (B) no. 17K14351, Grant-in-Aid for Scientific Research no. 16H05990 from the Japan Society for the Promotion of Science (JSPS), and PRESTO no. JPMJPR177A from the Japan Science and Technology Agency (JST). M.H. was supported as a JSPS international research fellow (no. 18F18804). **Author contributions:** T.K. and Y.To. conceived the project. T.K., A.K., and Y.Ta. grew the single crystals of Gd_2PdSi_3. T.K. characterized the magnetic and transport properties of the samples with the help of M.H. and A.K. T.N., Y.Y., H.S., H.N., and T.A. performed the resonant x-ray diffraction measurement. T.K., T.N., M.H., T.A., and Y.To. jointly discussed the result and wrote the manuscript with contributions from all authors. **Competing interests:** The authors declare no competing interests. **Data and materials availability:** Data reported in this paper are archived in Zenodo (*46*).

SUPPLEMENTARY MATERIALS

science.sciencemag.org/content/365/6456/914/suppl/DC1
Materials and Methods
Supplementary Text
Figs. S1 to S9
References (*47*–*54*)

7 May 2018; accepted 30 July 2019
Published online 8 August 2019
10.1126/science.aau0968

Skyrmion lattice with a giant topological Hall effect in a frustrated triangular-lattice magnet

Takashi Kurumaji, Taro Nakajima, Max Hirschberger, Akiko Kikkawa, Yuichi Yamasaki, Hajime Sagayama, Hironori Nakao, Yasujiro Taguchi, Taka-hisa Arima and Yoshinori Tokura

Science **365** (6456), 914-918.
DOI: 10.1126/science.aau0968originally published online August 8, 2019

Skyrmions in a frustrated magnet

Skyrmions—tiny, topologically protected whirlpools of spin—have been investigated as potential information carriers in spintronic devices. Usually, skyrmions appear in noncentrosymmetric materials or at interfaces between materials. In contrast to this rule of thumb, Kurumaji *et al.* observed a skyrmion lattice phase in the centrosymmetric material Gd_2PdSi_3. The magnetic frustration present in this material helped stabilize the skyrmion phase, which was detected through transport measurements in magnetic field.

Science, this issue p. 914